Nuclear Engineering and Technology 53 (2021) 4179–4188

Contents lists available at ScienceDirect

Nuclear Engineering and Technology

journal homepage: www.elsevier.com/locate/net

Original Article

Optimal earthquake intensity measures for probabilistic seismic demand models of ARP1400 reactor containment building

Duy-Duan Nguyen [a], Bidhek Thusa [b], Md Samdani Azad [b], Viet-Linh Tran [a], Tae-Hyung Lee [b, *]

[a] Department of Civil Engineering, Vinh University, Vinh 461010, Viet Nam
[b] Department of Civil and Environmental Engineering, Konkuk University, Seoul 05029, South Korea

A R T I C L E I N F O

Article history:
Received 19 April 2021
Received in revised form
16 June 2021
Accepted 20 June 2021
Available online 22 June 2021

Keywords:
Reactor containment building
Earthquake intensity measure
Nonlinear time-history analysis
Probabilistic seismic demand model
Optimality
Fragility curve

A B S T R A C T

This study identifies efficient earthquake intensity measures (IMs) for seismic performances and fragility evaluations of the reactor containment building (RCB) in the advanced power reactor 1400 (APR1400) nuclear power plant (NPP). The computational model of RCB is constructed using the beam-truss model (BTM) for nonlinear analyses. A total of 90 ground motion records and 20 different IMs are employed for numerical analyses. A series of nonlinear time-history analyses are performed to monitor maximum floor displacements and accelerations of RCB. Then, probabilistic seismic demand models of RCB are developed for each IM. Statistical parameters including coefficient of determination (R^2), dispersion (i.e. standard deviation), practicality, and proficiency are calculated to recognize strongly correlated IMs with the seismic performance of the NPP structure. The numerical results show that the optimal IMs are spectral acceleration, spectral velocity, spectral displacement at the fundamental period, acceleration spectrum intensity, effective peak acceleration, peak ground acceleration, A95, and sustained maximum acceleration. Moreover, weakly related IMs to the seismic performance of RCB are peak ground displacement, root-mean-square of displacement, specific energy density, root-mean-square of velocity, peak ground velocity, Housner intensity, velocity spectrum intensity, and sustained maximum velocity. Finally, a set of fragility curves of RCB are developed for optimal IMs.

1. Introduction

Worldwide seismic design codes and seismic structural analysis procedures have commonly been using peak ground acceleration (PGA) or spectral acceleration (S_a) as the seismic intensity measure (IM). Also, these IMs are widely employed for the seismic fragility assessment of infrastructures. Numerous studies were conducted to evaluate the interrelation between seismic IMs and seismic responses of buildings [1–3], bridges [4–6], on-ground liquid storage tanks [7], tunnels [8,9], and pipelines [10]. The aforesaid studies demonstrated that PGA and S_a are not always the best IMs for the seismic response evaluation and fragility analysis of civil engineering structures. Identifying optimal earthquake IMs for probabilistic seismic risk analysis of nuclear power plant (NPP) structures is necessary for the sake of efficiency and reliability of the analysis.

So far, several studies have investigated the correlation between IMs and seismic damage of NPP structures using the lumped-mass stick model (LMSM). Li et al. [11] calculated the correlation between IMs and seismic damage of a Canada Deuterium Uranium (CANDU) containment structure. They pointed out that S_a and S_d both at the fundamental period, T_1, are the strongest IMs. Recently, Nguyen et al. [12] performed time-history analyses to recognize the strongly correlated IMs for non- and base-isolated NPP structures considering high-frequency ground motions. They concluded that the significant IMs for low- and high-frequency earthquakes are different. However, LMSM is the simplest form of the structural model and is limited to simulate fundamental vibrational models and often linear analysis. Therefore, it is required to identify optimal earthquake IMs for seismic risk assessment of reactor containment building (RCB) in Advanced Power Reactor 1400 MWe (APR1400) NPPs using a practical nonlinear and more accurate numerical model.

For conducting the seismic probabilistic risk assessment (SPRA) of NPP components, selecting a practical and proper method is crucial. A classical approach, namely the factor method, is widely

* Corresponding author.
E-mail address: thlee@konkuk.ac.kr (T.-H. Lee).

https://doi.org/10.1016/j.net.2021.06.034

used in the seismic risk assessment of nuclear components [13]. However, seismic fragility curves and the high-confident-of-low-probability-of-failure values are derived based on empirical engineering judgment factors, which may not sufficiently reflect the randomness and uncertainty in SPRA of NPP structures. Consequently, some typical methods, which are incremental dynamic analysis, maximum likelihood estimation, and regression, have been commonly applied for nuclear engineering structures. Some studies compared the fragility curves of NPP structures and equipment using different methods [14,15]. They claimed that there is a significant difference between fragility curves developed by different methods. Moreover, fragility curves were developed mostly for containment buildings of early reactor generations such as AP1000, Indian 700 MWe PHWR, and CANDU.

Numerous studies also evaluated the seismic performance and fragility of NPP structures and systems using the LMSM [16–18]. To overcome the limitations of LMSM, a full three-dimensional finite element method (3D FEM) is employed to evaluate nonlinear seismic responses and fragility of NPP components [19–21]. However, a nonlinear time history analysis of 3D FEM is very time-consuming [22]. Thus, it is impractical to perform SPRA of large-scale structures like RCB or auxiliary buildings. It is necessary to use an appropriate model, which can surmount the drawbacks of LMSM and 3D FEM, in conducting SPRA of NPP components.

The purpose of this study is to identify optimal IMs to develop probabilistic seismic demand models (PSDMs) of RCB in APR1400 NPPs. For that, 20 earthquake IMs are considered in developing PSDMs. The nonlinear numerical modeling of RCB is constructed using the beam-truss model in OpenSees. A set of 90 ground motion records, which contain a wide range of amplitudes, magnitudes, epicentral distances, significant durations, and predominant

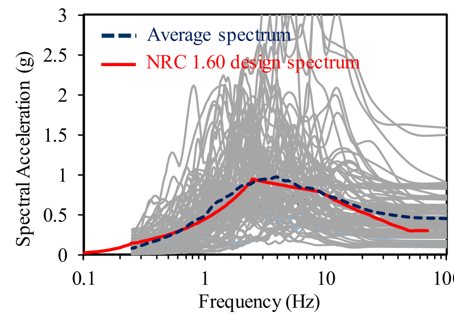

Fig. 1. Response spectra of selected ground motions.

Table 2
Statistical properties of selected ground motions.

Parameters	Min	Max	Mean	SD	COV
PGA (g)	0.093	1.585	0.453	0.272	0.601
PGA/PGV	0.250	3.294	1.088	0.614	0.565
Magnitude, M_w	5.2	7.8	6.63	0.513	0.077
Epicentral distance, R (km)	0.07	89.76	12.23	14.027	1.14
Significant duration, $D_{5\text{-}95}$ (s)	2.79	60.77	11.934	9.034	0.757
Predominant period, T_p (s)	0.04	1.24	0.374	0.202	0.540

Table 1
Earthquake intensity measures.

No.	Earthquake parameter	Definition	Unit	Reference
1	Peak ground acceleration	$PGA = \max\|a(t)\|$	g	–
2	Peak ground velocity	$PGV = \max\|v(t)\|$	m/s	–
3	Peak ground displacement	$PGD = \max\|d(t)\|$	m	–
4	Root-mean-square of acceleration	$A_{rms} = \sqrt{\frac{1}{t_{tot}}\int_0^{t_{tot}} a(t)^2 dt}$	g	Dobry et al. [28]
5	Root-mean-square of velocity	$V_{rms} = \sqrt{\frac{1}{t_{tot}}\int_0^{t_{tot}} v(t)^2 dt}$	m/s	Kramer [26]
6	Root-mean-square of displacement	$D_{rms} = \sqrt{\frac{1}{t_{tot}}\int_0^{t_{tot}} d(t)^2 dt}$	m	Kramer [26]
7	Arias intensity	$I_a = \frac{\pi}{2g}\int_0^{t_{tot}} a(t)^2 dt$	m/s	Arias [29]
8	Characteristic intensity	$I_c = (A_{rms})^{3/2}\sqrt{t_{tot}}$	$m^{1.5}/s^{2.5}$	Park et al. [30]
9	Specific energy density	$SED = \int_0^{t_{tot}} v(t)^2 dt$	m^2/s	–
10	Cumulative absolute velocity	$CAV = \int_0^{t_{tot}} \|a(t)\|dt$	m/s	Benjamin [31]
11	Acceleration spectrum intensity	$ASI = \int_{0.1}^{0.5} S_a(\xi = 0.05,\ T)dT$	g*s	Thun et al. [32]
12	Velocity spectrum intensity	$VSI = \int_{0.1}^{2.5} S_v(\xi = 0.05,\ T)dT$	m	Thun et al. [32]
13	Housner spectrum intensity	$HI = \int_{0.1}^{2.5} PS_v(\xi = 0.05,\ T)dT$	m	Housner [33]
14	Sustained maximum acceleration	SMA = the 3rd of PGA	g	Nuttli [34]
15	Sustained maximum velocity	SMV = the 3rd of PGV	m/s	Nuttli [34]
16	Effective peak acceleration	$EPA = \frac{mean(S_a^{0.1-0.5}(\xi = 0.05))}{2.5}$	g	Benjamin [31]
17	Spectral acceleration at T_1	$S_a(T_1)$	g	Shome et al. [35]
18	Spectral velocity at T_1	$S_v(T_1)$	m/s	–
19	Spectral displacement at T_1	$S_d(T_1)$	m	–
20	A95 parameter	$A_{95} = 0.764\ I_a^{0.438}$	g	Sarma & Yang [36]

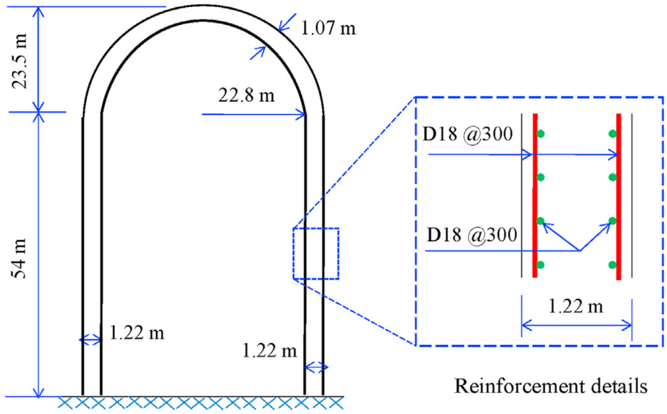

Fig. 2. Configuration of RCB.

periods, are utilized to perform nonlinear time-history analyses. Optimal IMs are recognized based on statistical indicators of PSDMs, which are the coefficient of determination, dispersion, practicality, and proficiency. Finally, seismic fragility curves of RCB with respect to optimal IMs are developed.

2. Backgrounds of PSDM and optimal intensity measures

2.1. Probabilistic seismic demand model

PSDM, which contains the relationship between structural demand and an earthquake IM, needs to be appropriately established in the probabilistic performance-based seismic design [3]. The most common expression of the relationship between seismic demand and earthquake IMs is the power form in Eq. (1) [4,5,23].

$$S_D = a \times (IM)^b \tag{1}$$

where S_D is the median value of structural demand; a and b are the regression coefficients; IM is the earthquake intensity measure considered. This equation can be rewritten in forms of linear regression as following

$$ln(S_D) = ln(a) + b \times ln(IM) \tag{2}$$

The conditional failure probability that the structural demand (D) exceeds its capacity for a given IM in the fragility analysis can be expressed as

$$P_f = P[D \geq d|IM] \tag{3}$$

where d is the specified value, normally it is based on the structural capacity. Assuming that the structural demand and capacity follow lognormal distributions, Eq. (3) can be rewritten as

$$P\left[D \geq d\middle|IM\right] = 1 - \Phi\left[\frac{ln(d) - ln(S_D)}{\sigma_{D|IM}}\right] \tag{4}$$

where $\Phi[-]$ is the standard normal function and $\sigma_{D|IM}$ is the logarithmic standard deviation.

2.2. Indicators for evaluating an optimal IM

In this study, four statistical properties, namely, the coefficient of determination, efficiency, practicality, and proficiency, are used

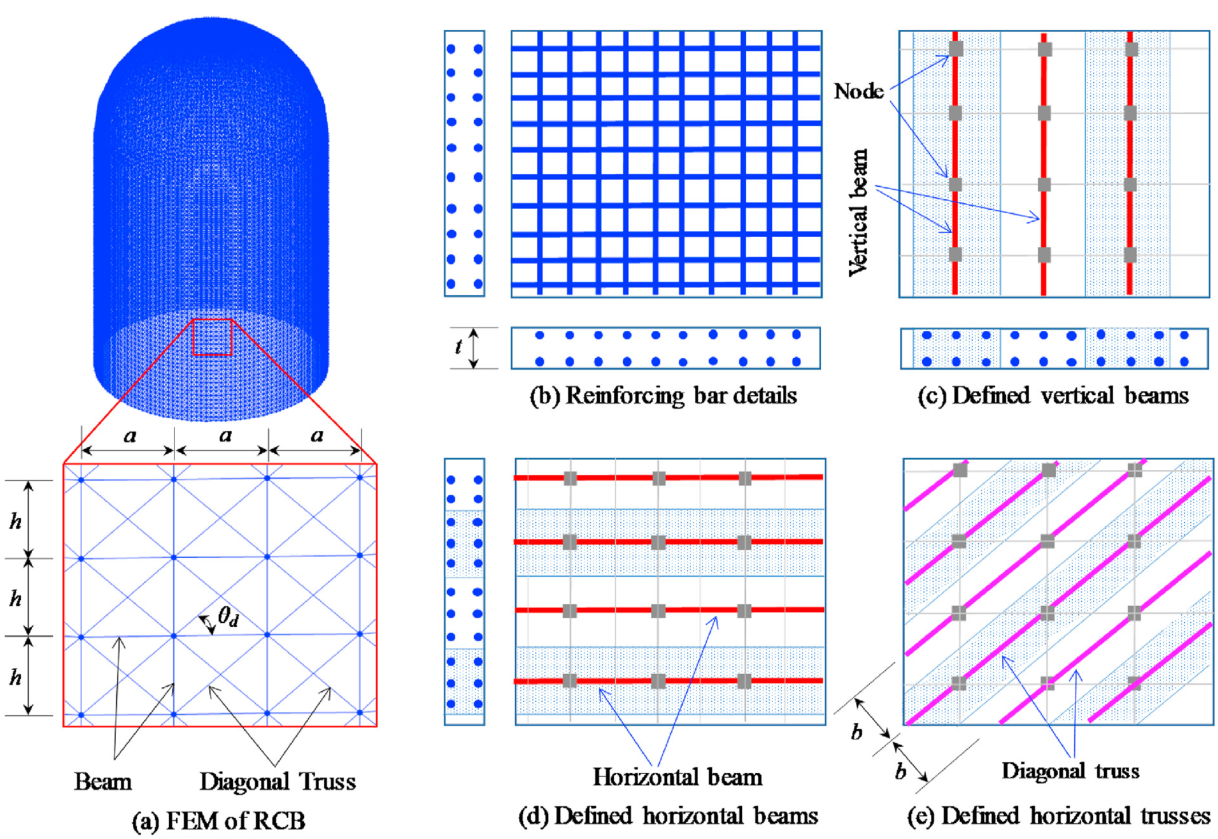

Fig. 3. Beam-truss model scheme of RCB.

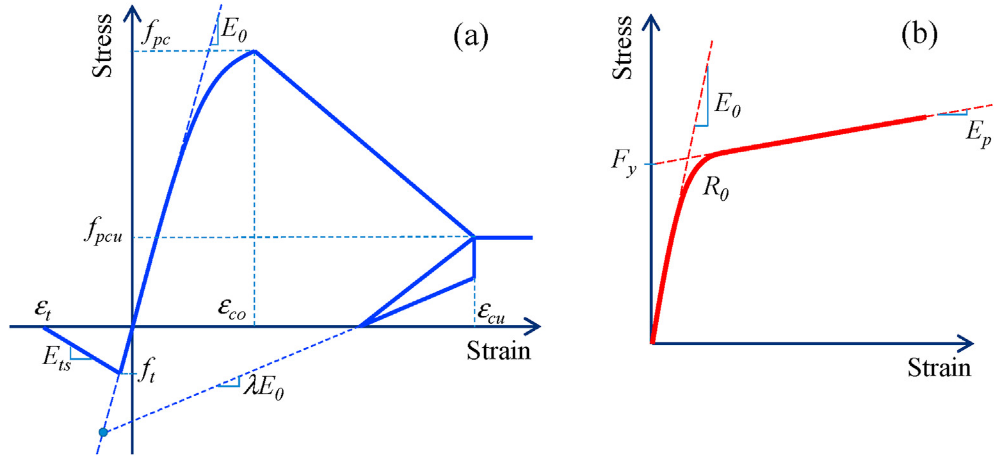

Fig. 4. Constitutive models of material: (a) concrete and (b) reinforcing bars.

for evaluating optimal IMs. These parameters have been utilized in the seismic risk evaluation of civil engineering structures [4,24,25]. Each indicator is described in this section.

2.2.1. Coefficient of determination (R^2)

The coefficient of determination, R^2, provides the proportion of the variance of one variable that can be predicted from the other variable. For PSDMs, R^2 denotes the percentage of the data that is the closest to the regression line (i.e. the best fit line). The closer R^2 value is to unity, the more significant the regression model is. It can be evaluated as

$$R^2 = \left(\frac{n(\sum x_i y_i) - (\sum x_i)(\sum y_i)}{\sqrt{\left[n\sqrt{x_i^2} - (\sum x_i)^2\right]\left[n\sqrt{y_i^2} - (\sum y_i)^2\right]}} \right)^2 \tag{5}$$

where n is the number of analysis data, x_i and y_i are the results of IMs and structural demand data, respectively.

2.2.2. Efficiency

The efficiency indicator is evaluated by the dispersion of regression fit for engineering demand parameters (EDPs) and each IM. In other words, the efficiency is measured in terms of the standard deviation of the scatterings of the PSDM, referred as $\sigma_{D|IM}$. The less scattered the data is, the more efficient IM is. The equation for calculating *efficiency* (i.e. standard deviation) can be expressed as

$$\sigma_{D|IM} = \sqrt{\frac{\sum\left(ln(d_i) - ln\left(a \times IM^b\right)\right)^2}{n-2}} \tag{6}$$

2.2.3. Practicality

The practicality represents the correlation between an IM and EDPs. This property is quantified by the regression model parameter, b (i.e. the slope of the regression line), as described in Eq. (2). The lower the value of b is, the less practical IM is.

2.2.4. Proficiency

Padgett et al. [4] proposed an indicator, namely proficiency, which can balance the selections between efficiency and practicality. The proficiency is defined by the ratio of dispersion ($\sigma_{D|IM}$) to the practicality (b), as shown in Eq. (7). The smaller the proficiency is, the more proficient PDSM is.

$$\xi = \frac{\sigma_{D|IM}}{b} \tag{7}$$

3. Earthquake intensity measures and input ground motions

3.1. Intensity measures

Earthquake IMs are fundamental for describing the important characteristics of ground motion quantitatively. Many IMs have

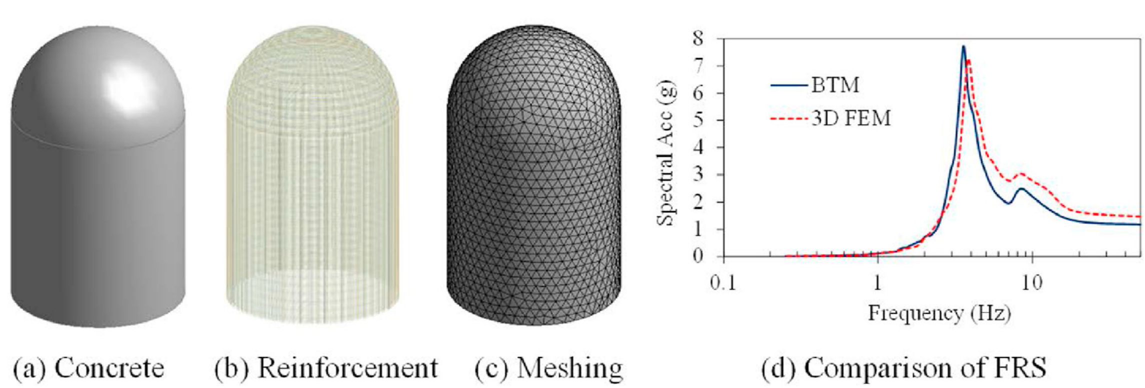

Fig. 5. 3D FEM and example of comparison of FRS with that of BTM.

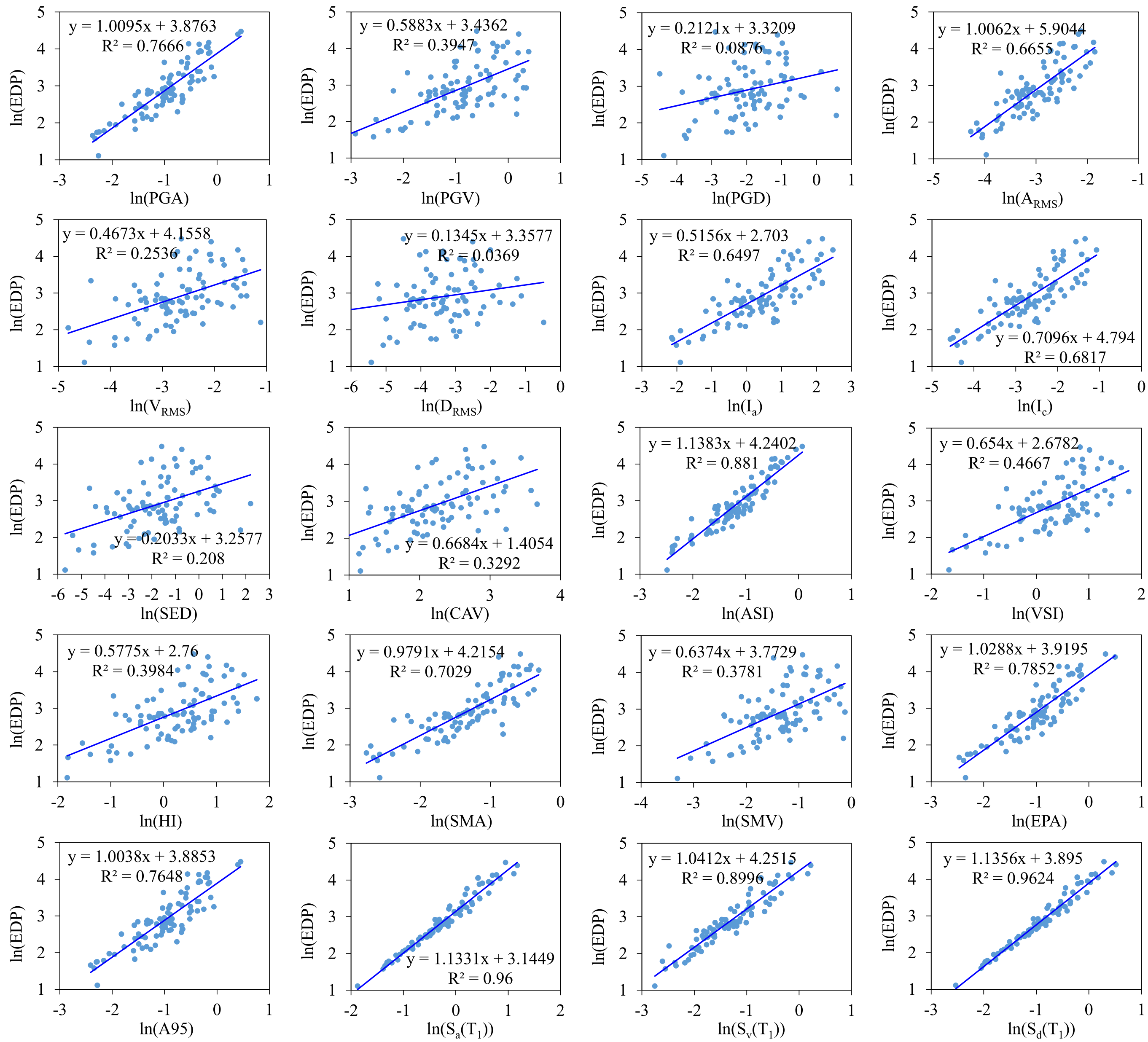

Fig. 6. PSDM for displacement with various IMs.

been proposed to characterize the amplitude, frequency content, and duration of motions [26]. To obtain the seismic IMs, a direct evaluation from earthquake accelerograms and a calculation by the software can be implemented. This study accounts for 20 common ground motion IMs and these parameters are calculated for every motion record using SeismoSignal [27]. The used IMs are described in Table 1. It should be noted that T_1 in this table is the fundamental period of the structure.

3.2. Input ground motions

A set of 90 ground motion records are selected from historic earthquakes, which are available in the PEER center database [37]. A wide range of earthquake amplitudes, magnitudes, epicentral distances, significant durations, and predominant periods is considered in used ground motions whose response spectra are shown in Fig. 1. It should be noted that the mean spectrum of the input motions is comparable with the US Nuclear Regulatory Commission (NRC) 1.60 design spectrum [38]. The statistical parameters of the selected ground motions are presented in Table 2. Noting that SD and COV in Table 2 are abbreviations of standard deviation and coefficient of variation, respectively.

4. Numerical modeling of RCB

RCB is one of the most crucial structures in the APR1400 NPP. It is a reinforced concrete (RC) structure, which consists of a cylinder and a dome part. The cylinder radius and height are 23.5 m and 54.0 m, respectively, while the thickness of the cylinder wall is 1.22 m, as shown in Fig. 2. The dome radius is 23.2 m, and its average thickness is 1.07 m.

Generally, RCB is modeled by LMSM or 3D FEM to simulate its seismic performance. However, LMSM is too simple to simulate the nonlinear behavior of RCB and 3D-FEM is too expensive in terms of the CPU time. Therefore, an optimal model, namely the beam-truss model (BTM) is employed to perform nonlinear time-history

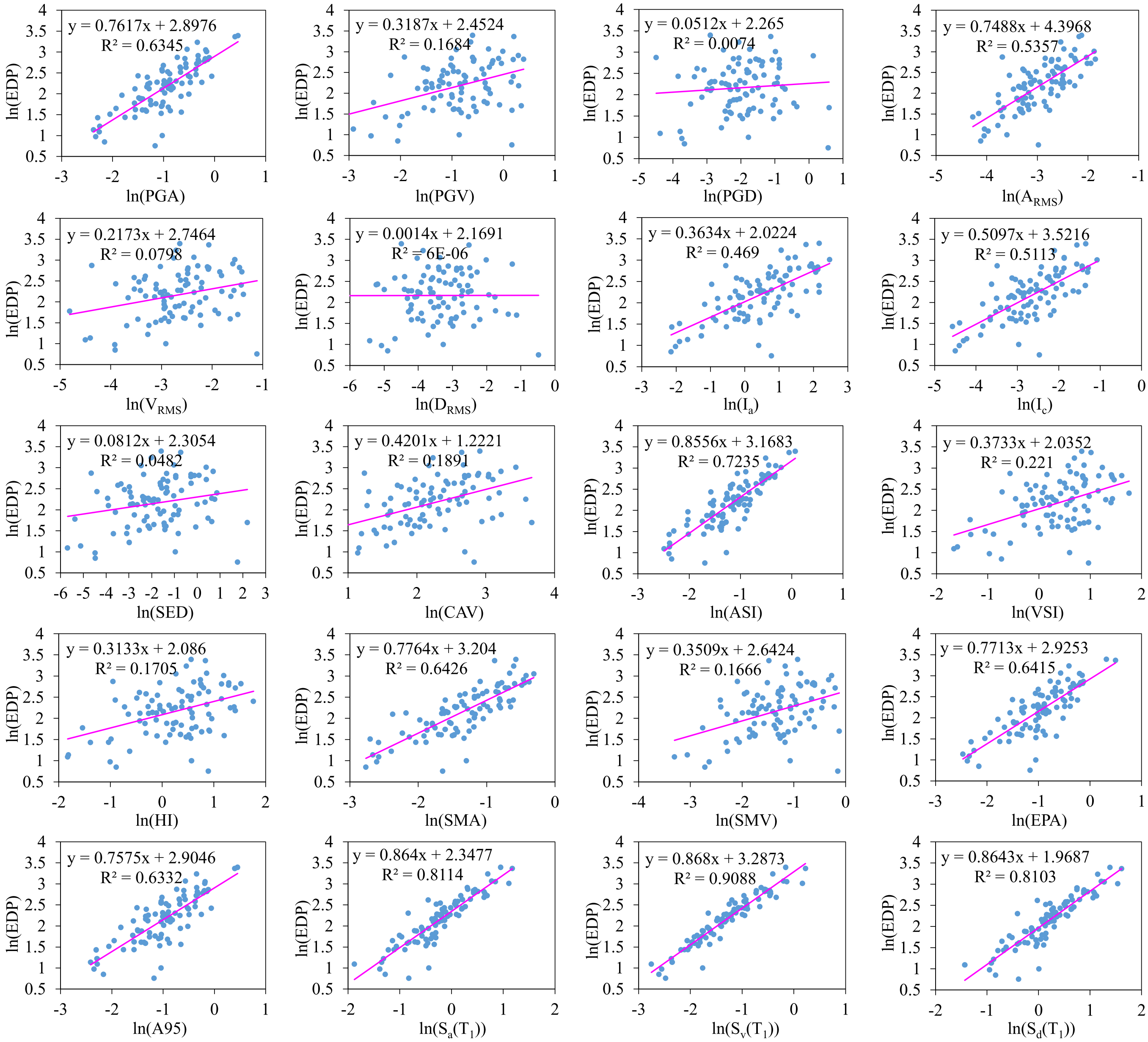

Fig. 7. PSDM for acceleration with various IMs.

analyses of RCB in this study. The efficiency of this modeling approach was highlighted in Nguyen et al. [22].

BTM consists of vertical and horizontal beam elements and diagonal truss elements, as shown in Fig. 3a. The rationality in simulating the RC wall of RCB with beam and truss elements can be expressed by the following points. (1) Shell stress resultants are computed by combining stresses from concrete and reinforcement layers. The horizontal and vertical normal stresses are attributed to the horizontal and vertical beams. Meanwhile, the shear stress of the wall is considered using diagonal truss elements, which are also able to represent the compressive and tensile behavior of concrete. (2) The nodes, where horizontal, vertical, and diagonal elements are intersected, have six degrees of freedom. It is the same as those of shell element nodes. Additionally, thorough verifications of this approach using experimental tests were conducted in previous studies [39,40].

RC cross-sections are applied for vertical and horizontal beam elements, whereas a pure concrete section is used for modeling the diagonal truss elements [39,40]. Fig. 3b–e shows the schematic modellings of the RCB wall in BTM. The length of beam and truss elements depends on the mesh size. In this study, the length of the horizontal and vertical beams is set to 1.0 m after conducting a mesh convergence test. Meanwhile, the width of the beam cross-section is exactly equal to the thickness of the RC wall (i.e., $t = 1.22$ m), and the height of the beam is set to the size of the panels. The width of the diagonal trusses (b) is the product of the panel length (a) and $\sin(\theta_d)$, expressed as

$$b = a \times \sin(\theta_d) \tag{8}$$

where θ_d is the angle between the horizontal and diagonal elements.

The BTM-based FE model of RCB is developed using OpenSees [41], a commonly used open-source platform for earthquake

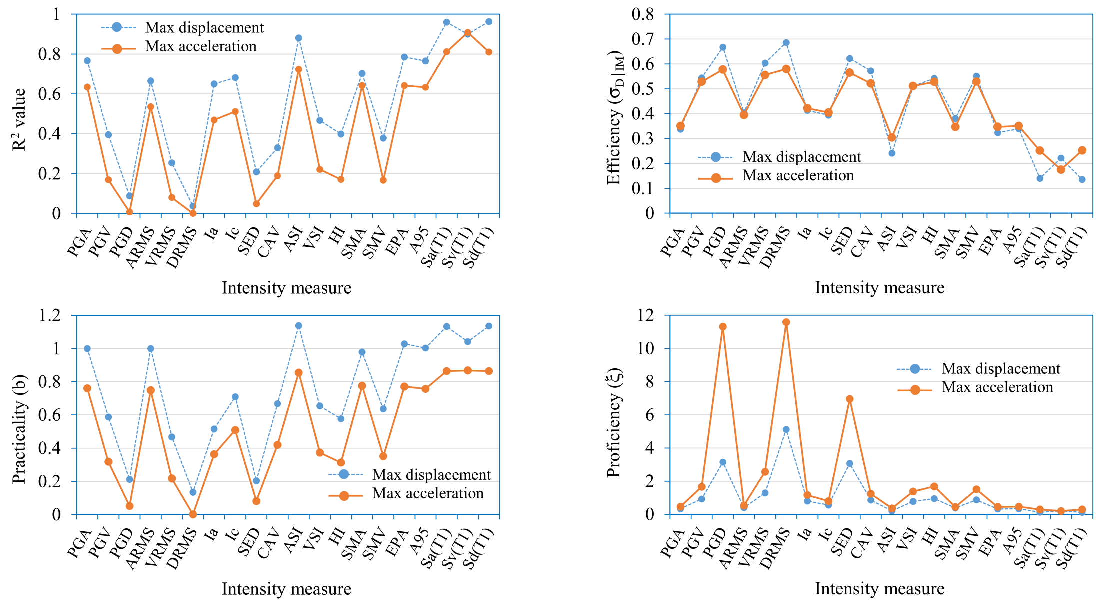

Fig. 8. Statistical indicators of PSDMs.

Table 3
Proposed damage states of RCB [22].

Damage state	Drift (%)	Description
DS1 (Minor)	0.01	Concrete cracking
DS2 (Moderate)	0.03	Rebar yielding
DS3 (Extensive)	0.15	Extensive cracking & yielding at the bottom
DS4 (Collapse)	0.23	Concrete crushing

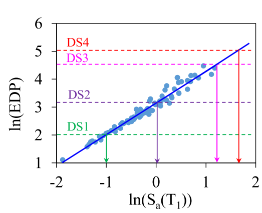

Fig. 9. Estimation of mean values for different damage states.

engineering simulation. For modeling nonlinear materials, the *concrete02* [42] and *steel02* models [43] are employed for modeling concrete and reinforcing bars, respectively, as shown in Fig. 4. The *forceBeamColumn* element associated with a fiber section model is used to model nonlinear behaviors of beam elements. Meanwhile, the *corotTruss* element is used for constructing the diagonal truss elements.

To verify the computational accuracy of BTM, a full 3D FEM is developed in ANSYS [44]. The nonlinear *solid187* and *beam188* element models are used for concrete and reinforcing bars, respectively. Whereas *conta174* is applied for modeling the contact between concrete and reinforcement. The model is meshed into 64,299 prism solid elements and 24,647 beam elements for concrete and reinforcing bars, respectively, after conducting a mesh-sensitivity analysis. Fig. 5a–c shows the concrete part and reinforcing bars in full 3D FEM. Nonlinear time-history analyses of the full 3D FEM are thereafter performed and their floor responses are compared. Fig. 5d shows an example of floor response spectra (FRS) at the top of the structure obtained from BTM and 3D FEM. The comparison emphasizes that the FRS from BTM and 3D FEM are in good agreement that verifies the accuracy of the BTM-based computational model.

5. PSDM results of RCB

To develop PSDMs and identify the optimal IMs, time-history analyses of the RCB model in the horizontal X-direction are performed using 90 ground motions, separately. The maximum floor displacements and accelerations are selected as engineering demand parameters (EDPs). Then, PSDMs of RCB are developed for all considered IMs and EDPs. The optimality of IMs is evaluated using statistical indicators of the PSDM, namely, the coefficient of determination (R^2), dispersion (i.e. standard deviation), practicality, and proficiency. The higher R^2 and practicality are, the more correlated and efficient IM is. Meanwhile, if the standard deviation and proficiency are lower, the considered IM is more efficient and vice versa.

Figs. 6 and 7 show the PSDMs of the RCB structure for 20 IMs using the maximum displacement and acceleration, respectively. It can be observed that PSDMs with respect to $S_a(T_1)$, $S_v(T_1)$, $S_d(T_1)$, ASI, EPA, PGA, A95, and SMA have a higher R^2 value than others. In other words, the scattering of PSDMs using the mentioned IMs is much smaller than that of others. Therefore, those IMs can be considered to be strongly correlated to the seismic damage of RCB. The trend is similar for both displacement and acceleration responses. Overall, the strongly correlated IMs are directly related to the acceleration. This observation can be attributed that the seismic response of a relatively rigid structure like RCB is sensitive to acceleration rather than velocity or displacement [12]. Moreover, $S_a(T_1)$, $S_v(T_1)$, and $S_d(T_1)$ are shown to be the strongest IMs since these parameters are combinations of ground motion (i.e. response spectra of earthquakes) and structural properties (i.e. fundamental period of the structure).

Fig. 8 presents four statistical parameters of PSDMs for 20 IMs. The efficiency of IMs is evaluated through the specified indicators. It is found that PSDMs with respect to $S_a(T_1)$, $S_v(T_1)$, and $S_d(T_1)$ have the lowest standard deviation and proficiency, and the largest R^2 and practicality, followed by ASI, EPA, PGA, A95, and SMA. Accordingly, these measures are considered as the optimal or

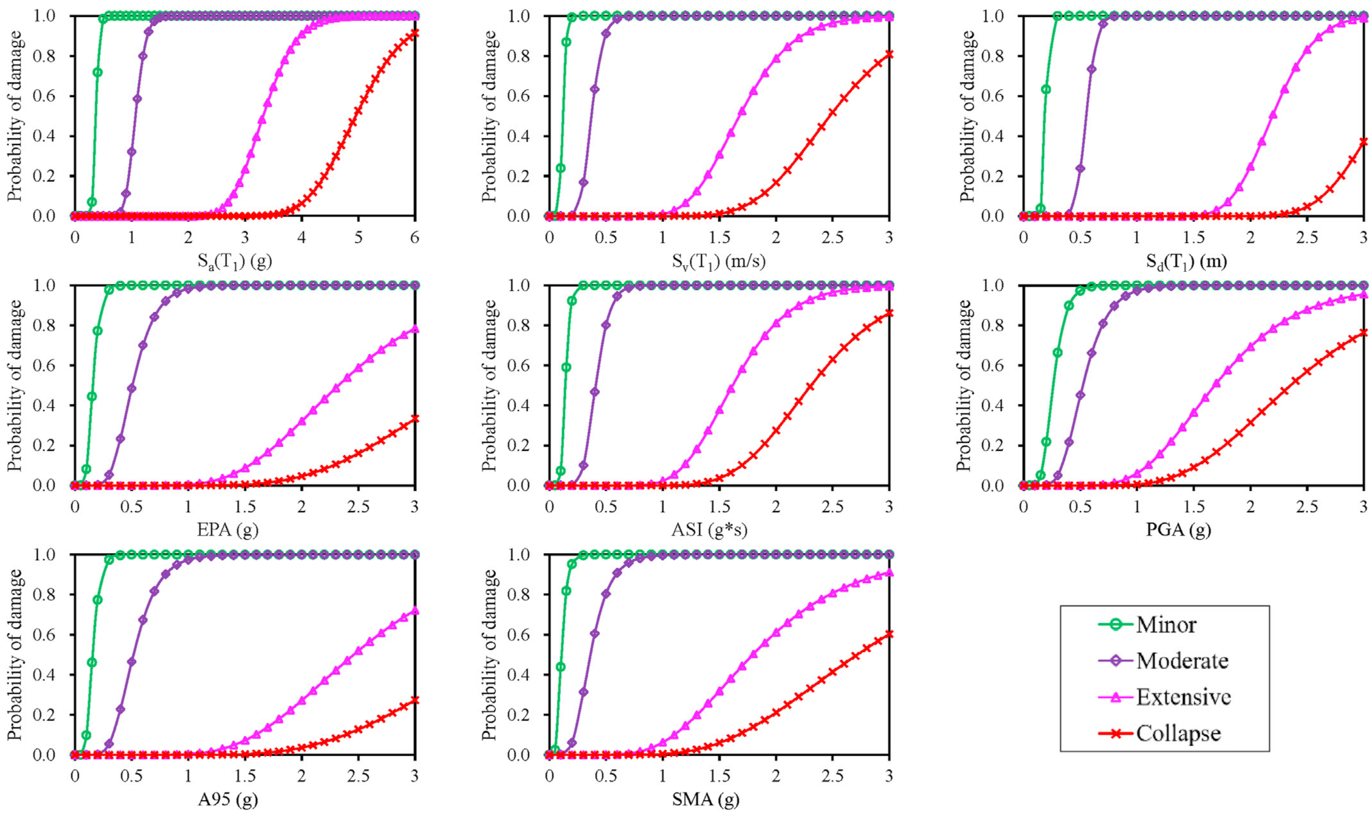

Fig. 10. Fragility curves of RCB with respect to optimal IMs.

Table 4
Fragility function parameters of RCB with various optimal IMs.

IM	Fragility function parameter	Damage state			
		Minor	Moderate	Extensive	Collapse
$S_a(T_1)$	Mean (g)	0.369	1.067	3.320	4.953
	SD	0.140	0.140	0.140	0.140
$S_v(T_1)$	Mean (m/s)	0.117	0.371	1.676	2.474
	SD	0.221	0.221	0.221	0.221
$S_d(T_1)$	Mean (m)	0.191	0.551	2.194	3.136
	SD	0.136	0.136	0.136	0.136
ASI	Mean (g*s)	0.142	0.408	1.617	2.309
	SD	0.241	0.241	0.241	0.241
EPA	Mean (g)	0.157	0.506	2.325	3.448
	SD	0.324	0.324	0.324	0.324
PGA	Mean (g)	0.260	0.521	1.685	2.354
	SD	0.338	0.338	0.338	0.338
A95	Mean (g)	0.155	0.515	2.457	3.679
	SD	0.339	0.339	0.339	0.339
SMA	Mean (g)	0.106	0.361	1.794	2.714
	SD	0.381	0.381	0.381	0.381

Table 5
Comparison of HCLPF values of the RCB structure between different studies.

Failure mode	KEPCO & KHNP [45]	Nguyen et al. [22]
Shear failure near the base	0.94g	0.81g

efficient IMs for PSDMs of the RCB structure. On the other hand, Fig. 8 indicates that the inefficient IMs for PSDMs of RCB are PGD, D_{RMS}, SED, V_{RMS}, PGV, HI, VSI, and SMV.

6. Derivation of fragility curves using PSDMs

For generating seismic fragility curves, a set of damage states and corresponding damage indices should be defined. This study adopts the damage states of the RCB structure proposed by Nguyen et al. [22] to develop fragility curves. Four damage states including minor (DS1), moderate (DS2), extensive (DS3), and collapse (DS4), were defined based on the nonlinear pushover analysis, as presented in Table 3.

To generate a fragility curve assumed to have a lognormal distribution, the mean and the standard deviation need to be defined. The standard deviations are already calculated in the previous section, while the mean of each damage state can be readily estimated based on the linear regression in the previous section, as illustrated in Fig. 9. Seismic fragility curves of RCB with respect to each of the optimal IMs, $S_a(T_1)$, $S_v(T_1)$, $S_d(T_1)$, ASI, EPA, PGA, A95, and SMA, are shown in Fig. 10. The authors suggest that a seismic fragility curve with respect to an optimal IM is more reliable than that of a less relevant IM. The means and standard deviations of the proposed fragility curves are shown in Table 4. This family of fragility curves can be readily applied for the probabilistic seismic risk assessment of the APR1400 reactor containment buildings.

The conservative deterministic failure margin (CDFM) method is commonly employed to estimate the seismic capacity of NPP structures. KEPCO & KHNP [45] used CDFM to calculate the high confidence of low probability of failure (HCLPF) of the containment structure. They pointed out that the failure mode of RCB is shear failure near the base, which is corresponding to damage state 4 (DS4) defined in the study of Nguyen et al. [22]. Table 5 shows a comparison of HCLPF values, which were calculated by KEPCO & KHNP [45] and Nguyen et al. [22]. It is found that the seismic capacity based on the estimation of Nguyen et al. [22] is slightly lower than that of KEPCO & KHNP [45]. This observation can be attributed to the reason that the effects of pre-stressed tendons on the structural capacity were not considered in the numerical model of Nguyen et al.[22]. Therefore, the adopted damage states in Table 3 and corresponding median seismic intensity values estimated in Fig. 9 and Table 4 might be slightly conservative.

7. Conclusions

This study developed PSDMs for various IMs and identified optimal IMs for the seismic performance of the RCB structure in APR1400 NPPs. A group of 90 ground motion records and 20 different IMs were used in nonlinear time-history analyses. A set of fragility curves were generated with respect to optimal IMs based on developed PSDMs. The following conclusions are drawn.

- The optimal IMs for PSDMs of the RCB structure are $S_a(T_1)$, $S_v(T_1)$, and $S_d(T_1)$ followed by ASI, EPA, PGA, A95, and SMA. The PSDMs with respect to these IMs contain higher values of R^2, lower standard deviations and proficiency values, and larger practicalities than those of others. Mostly, the optimal IMs are directly related to the acceleration.
- The less efficient IMs for PSDMs of RCB are PGD, D_{RMS}, SED, V_{RMS}, PGV, HI, VSI, and SMV. These IMs are displacement- and velocity-based parameters.
- A set of fragility curves of RCB are developed for the optimal IMs. These curves can be useful in the probabilistic seismic risk assessment of the RCB structure in APR1400 NPPs. Since the influences of pre-stressed tendons are not considered in the numerical model, the obtained result might be slightly conservative.

Declaration of competing interest

The authors declare that they have no known competing financial interests or personal relationships that could have appeared to influence the work reported in this paper.

Acknowledgement

This research is supported by the Korea Institute of Energy Technology Evaluation and Planning (KETEP) and the Ministry of Trade, Industry & Energy (MOTIE) of the Republic of Korea (No. 20201510100020).

References

[1] A. Elenas, K. Meskouris, Correlation study between seismic acceleration parameters and damage indices of structures, Eng. Struct. 23 (6) (2001) 698–704.
[2] K. Kostinakis, A. Athanatopoulou, K. Morfidis, Correlation between ground motion intensity measures and seismic damage of 3D R/C buildings, Eng. Struct. 82 (2015) 151–167.
[3] J.R. Pejovic, N.N. Serdar, R.R. Pejovic, Optimal intensity measures for probabilistic seismic demand models of RC high-rise buildings, Earthq. Struct. 13 (3) (2017) 221–230.
[4] J.E. Padgett, B.G. Nielson, R. DesRoches, Selection of optimal intensity measures in probabilistic seismic demand models of highway bridge portfolios, Earthq. Eng. Struct. Dynam. 37 (5) (2008) 711–725.
[5] V. Jahangiri, M. Yazdani, M.S. Marefat, Intensity measures for the seismic response assessment of plain concrete arch bridges, Bull. Earthq. Eng. 16 (9) (2018) 4225–4248.
[6] C. Zelaschi, R. Monteiro, R. Pinho, Critical assessment of intensity measures for seismic response of Italian RC bridge portfolios, J. Earthq. Eng. 23 (6) (2019) 980–1000.
[7] H.N. Phan, F. Paolacci, Efficient intensity measures for probabilistic seismic response analysis of anchored above-ground liquid steel storage tanks, in: Pressure Vessels and Piping Conference, American Society of Mechanical Engineers, 2016.
[8] Z. Chen, J. Wei, Correlation between ground motion parameters and lining damage indices for mountain tunnels, Nat. Hazards 65 (3) (2013) 1683–1702.
[9] D.D. Nguyen, D. Park, S. Shamsher, V.Q. Nguyen, T.H. Lee, Seismic vulnerability assessment of rectangular cut-and-cover subway tunnels, Tunn. Undergr. Space Technol. 86 (2019) 247–261.
[10] H. Shakib, V. Jahangiri, Intensity measures for the assessment of the seismic response of buried steel pipelines, Bull. Earthq. Eng. 14 (4) (2016) 1265–1284.
[11] C. Li, C. Zhai, S. Kunnath, D. Ji, Methodology for selection of the most damaging ground motions for nuclear power plant structures, Soil Dynam. Earthq. Eng. 116 (2019) 345–357.
[12] D.D. Nguyen, B. Thusa, T.S. Han, T.H. Lee, Identifying significant earthquake intensity measures for evaluating seismic damage and fragility of nuclear power plant structures, Nucl. Eng. Technol. 52 (1) (2020) 192–205.
[13] EPRI, Methodology for Developing Seismic Fragilities, Report TR-103959, Palo Alto, CA, USA, 1994.
[14] T.K. Mandal, S. Ghosh, N.N. Pujari, Seismic fragility analysis of a typical Indian PHWR containment: comparison of fragility models, Struct. Saf. 58 (2016) 11–19.
[15] T.T. Tran, A.T. Cao, T.H.X. Nguyen D. Kim, Fragility assessment for electric cabinet in nuclear power plant using response surface methodology, Nucl. Eng. Technol. 51 (3) (2019) 894–903.
[16] I.K. Choi, Y.S. Choun, S.M. Ahn, J.M. Seo, Probabilistic seismic risk analysis of CANDU containment structure for near-fault earthquakes, Nucl. Eng. Des. 238 (6) (2008) 1382–1391.
[17] Y.N. Huang, A.S. Whittaker, N. Luco, A probabilistic seismic risk assessment procedure for nuclear power plants: (II) Application, Nucl. Eng. Des. 241 (9) (2011) 3985–3995.
[18] J.W. Jung, H.W. Jang, J.H. Kim, J.W. Hong, Effect of second hardening on floor response spectrum of a base-isolated nuclear power plant, Nucl. Eng. Des. 322 (2017) 138–147.
[19] X. Bao, M.H. Zhang, C.H. Zhai, Fragility analysis of a containment structure under far-fault and near-fault seismic sequences considering post-mainshock damage states, Eng. Struct. 198 (2019) 109511.
[20] D. Wang, C. Wu, Y. Zhang, Z. Ding, W. Chen, Elastic-plastic behavior of AP1000 nuclear island structure under mainshock-aftershock sequences, Ann. Nucl. Energy 123 (2019) 1–17.
[21] C. Zhao, N. Yu, Y. Oz, J. Wang, Y.L. Mo, Seismic fragility analysis of nuclear power plant structure under far-field ground motions, Eng. Struct. 219 (2020) 110890.
[22] D.D. Nguyen, B. Thusa, H. Park, M.S. Azad, T.H. Lee, Efficiency of various structural modelling schemes on evaluating seismic performance and fragility of APR1400 containment building, Nucl. Eng. Technol. (2021), https://doi.org/10.1016/j.net.2021.02.006. In press.
[23] C.A. Cornell, F. Jalayer, R.O. Hamburger, D.A. Foutch, Probabilistic basis for 2000 SAC federal emergency management agency steel moment frame guidelines, J. Struct. Eng. 128 (4) (2002) 526–533.
[24] N. Luco, C.A. Cornell, Structure-specific scalar intensity measures for near-source and ordinary earthquake ground motions, Earthq. Spectra 23 (2) (2007) 357–392.
[25] P. Giovenale, C.A. Cornell, L. Esteva, Comparing the adequacy of alternative ground motion intensity measures for the estimation of structural responses, Earthq. Eng. Struct. Dynam. 33 (8) (2004) 951–979.
[26] S.L. Kramer, Geotechnical Earthquake Engineering, Prentice Hall. Inc., Upper Saddle River, New Jersey, USA, 1996.
[27] SeismoSignal - a computer program for signal processing of strong-motion data, available from, http://www.seismosoft.com, 2017.
[28] R. Dobry, I.M. Idriss, E. Ng, Duration characteristics of horizontal components of strong-motion earthquake records, Bull. Seismol. Soc. Am. 68 (5) (1978) 1487–1520.
[29] A. Arias, M*easure of Earthquake Intensity*, Massachusetts Inst. of Tech., Cambridge. Univ. of Chile, Santiago de Chile, 1970.
[30] Y.J. Park, A.H.S. Ang, Y.K. Wen, Seismic damage analysis of reinforced concrete buildings, J. Struct. Eng. 111 (4) (1985) 740–757.
[31] J.R. Benjamin, A Criterion for Determining Exceedance of the Operating Basis Earthquake, Report No. EPRI NP-5930, Electrical Power Research Institute, Palo Alto, California, USA, 1988.
[32] V. Thun, Earthquake ground motions for design and analysis of dams, in: Earthquake Engineering and Soil Dynamics II-Recent Advances in Ground-Motion Evaluation, 1988.
[33] G.W. Housner, Spectrum intensities of strong-motion earthquakes, in: Symposium on Earthquake and Blast Effects on Structures, Los Angeles, California, USA, 1952.
[34] O.W. Nuttli, The Relation of Sustained Maximum Ground Acceleration and Velocity to Earthquake Intensity and Magnitude, US Army Engineer Waterways Experiment Station, Vicksburg, Mississippi, USA, 1979.
[35] N. Shome, C.A. Cornell, P. Bazzurro, J.E. Carballo, Earthquakes, records, and nonlinear responses, Earthq. Spectra 14 (3) (1998) 469–500.
[36] S.K. Sarma, K.S. Yang, An evaluation of strong motion records and a new parameter A95, Earthq. Eng. Struct. Dynam. 15 (1) (1987) 119–132.
[37] PEER ground motion database. http://peer.berkeley.edu/peer_ground_motion_database, 2019.
[38] RG 1.60, Design Response Spectra for Seismic Design of Nuclear Power Plants, 1.60, Regulatory Guide, Rockville, Maryland, USA, 2014. Revision 2.
[39] Y. Lu, M. Panagiotou, I. Koutromanos, Three-dimensional beam-truss model for reinforced concrete walls and slabs–part 1: modeling approach,

validation, and parametric study for individual reinforced concrete walls, Earthq. Eng. Struct. Dynam. 45 (9) (2016) 1495–1513.
[40] Y. Lu, M. Panagiotou, Three-dimensional beam–truss model for reinforced concrete walls and slabs–part 2: modeling approach and validation for slabs and coupled walls, Earthq. Eng. Struct. Dynam. 45 (11) (2016) 1707–1724.
[41] S. Mazzoni, F. McKenna, M.H. Scott, G.L. Fenves, OpenSees Command Language Manual, Pacific Earthquake Engineering Research, PEER) Center, Berkeley, CA, USA, 2006.
[42] D.C. Kent, R. Park, Flexural members with confined concrete, J. Struct. Division 97 (7) (1971) 1969–1990.
[43] M. Menegotto, P.E. Pinto, Method of analysis for cyclically loaded reinforced concrete plane frames including changes in geometry and non-elastic behavior of elements under combined normal force and bending, in: IABSE Sym. Of Resist. and Ult. Deform. of Struct. Acted on by Well-Defined Repeat, Loads, Lisbon, Portugal, 1973.
[44] ANSYS, ANSYS Mechanical APDL Element Reference, 2019.
[45] KEPCO & KHNP, APR1400 Standard Design Certification Application Design Control Document, 2018. Revision 3, Tier 2 (Chapter 19).